Eurographics Workshop on Visual Computing for Biology and Medicine (2014)
I. Viola, K. Bühler, and T. Ropinski (Editors)

Imaging the vascular network of the human spleen from immunostained serial sections

Christine Ulrich[1], Oleg Lobachev[2], Birte Steiniger[3], and Michael Guthe[2]

[1] Technical Workshop, Psychology Faculty, Philipps-University Marburg, Germany
[2] Visual Computing, University Bayreuth, Germany
[3] Institute for Anatomy and Cell Biology, Medical Faculty, Philipps-University Marburg, Germany

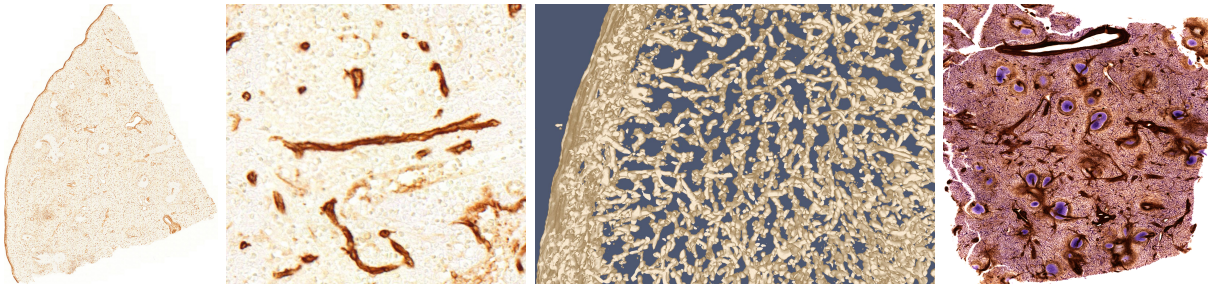

Figure 1: From left to right: One slide of an immunostained specimen of the human spleen stained for CD34 occurring endothelial cells of capillaries and larger blood vessels and in a small fibroblast population; the scan resolution is 25856×32000. Detail of the slide showing the stained capillaries. Detail of the iso-surface reconstruction from the aligned serial sections. Volume rendering of a further spleen immunostained for CD34, smooth muscle alpha actin and CD271 (first two targets colored brown, the latter one colored blue), both aligned with our technique.

Abstract

The spleen is one of the organs, where the micro-structure and the function on that level are not completely understood. It was for example only recently found that is has an open circulation, which distinguishes it from all other organs. Imaging the complete vascular network from the arteries to open-ended capillaries would greatly facilitate research in this area.

The structure of such tissue is best uncovered using immunehistological staining. This can however only be applied to thin tissue sections and larger structures span several slices. Due to the deformation induced when cutting the specimen, standard registration algorithms cannot be used to merge the images into a volume.

We propose a specialized matching algorithm to robustly determine corresponding regions in the images. After a rigid alignment of the scans, we use a cubic B-spline to deform and align the images. During this process we minimize the total deformation to produce as accurate results as possible.

Categories and Subject Descriptors (according to ACM CCS): I.4.3 [Image Processing and Computer Vision]: Enhancement—Registration

1. Introduction

Imaging blood vessels, nerves or other mesoscopic structures has several applications in biology and anatomy. Such structures may span regions of one or several millimeters and specimen of such size need to be digitized as a whole. On the other hand, small structures of less than 1 μm are also important to understand the structure and function of the tissue. Therefore, only microscopy based approaches are applicable in this context.

Our methods aim at providing insights into the course of

DOI: 10.2312/vcbm.20141185

arterial blood vessels in the human spleen. The spleenic vascular network is open: the capillaries have open ends and no connections to the venous sinuses. Thus, the blood flows through the connective tissue without any separating wall and – interestingly – without clotting. This behavior is believed to be unique to the spleen, signifying the importance of the study of its blood vessel system. In addition, the human spleen has specialized capillary vessels (called sheathed capillaries), which do not occur in any other organ. The location, shape and function of these vessels need to be clarified. Our goal is to enable answers to these questions by depicting the shape of the vessels in an aligned stack of serial sections. Registered serial sections are then used to obtain volume or mesh data of the capillary network. It does not make sense to regard a single slide, as it is too thin to contain blood vessels connected at a mesoscopic dimension.

Injections or genetic modifications, which are commonly used in biological models, are not possible in humans. As a consequence, staining of specific cells to discriminate them, has to be performed after removal of the specimen. The only applicable technique that is versatile enough, is immunohistological staining. Unfortunately, staining substances do not penetrate a specimen further than a few micrometers. Despite recent advances in confocal microscopy, it is therefore not possible to examine specimens with a thickness of more than approximately 50 μm using immunostaining. The only technique left is preparing 5–10 μm thick serial sections. This allows immunohistological staining, but disassembles the overall structure in mesoscopic dimension and produces deformations. As a result aligning the sections and reconstructing the volume is needed. Series with up to 400 sections are possible, amounting to a total thickness of up to 4 *mm*. Smaller series with up to 50 sections are simpler to produce and we thus currently work with this range. Our techniques are however applicable to these larger series as well.

So far only small details of serial sections have been used to examine blood vessels or nerves. With the recent introduction of automated slide scanning microscopes, large serial sections can be digitized with high resolution. However, the special properties of serial sections pose several challenges for such a reconstruction, which we will discuss in the following.

1.1. Immunohistological Staining

Immunohistological staining is a procedure to detect proteins or other antigens in thin sections of tissue that have been either fixed and embedded in paraffin or a similar material for cutting with a microtome. Alternatively, frozen sections may be used. There are different detection systems available. The system used for our experiments is called the "ABC"-system (avidin-biotinylated peroxidase complex system).

For processing of the sections the embedding material needs to be removed in a first step. Then appropriate antigen retrieval is performed and endogenous biotin and peroxidase activity is blocked. We first use a specific antibody, which binds to the surface and/or the interior of the cut cell. Then a second antibody binding to the first one is subsequently applied. This secondary antibody has been conjugated to the small molecule biotin. Biotin is used, because it is bound by the protein avidin at one of the highest affinities known in biological systems. To detect the biotin-labeled secondary antibody, we using a molecular complex of avidin and biotinylated peroxidase containing many unoccupied biotin-binding sites in the avidin molecules.

When the molecular complex is applied to the sections, it binds to the biotin of the secondary antibodies. This means, that many peroxidase molecules are present at the site of the antigen. Peroxidase is an enzyme which catalyzes an oxidative polymerization of soluble color substances such as diaminobenzidine to an insoluble product in the presence of hydrogen peroxide. Thus, a permanent brown precipitate is deposited, where the enzyme has exerted its function at the location of the first antibody.

After sealing the stained section it with a cover slip, the slide can be scanned for further digital processing. Figure 1, left, shows a detail of a scanned immunostained specimen using diaminobenzidine (brown) only. This staining designates capillary endothelial cells, blood stem cells, and certain fibroblasts in the spleen. We use it to visualize the vascular network. Some specimen (like Figure 1, right) are also immunostained for further targets, shown in brown and blue color. In our experiments, we utilize CD34 immunostaining as a standard.

We used a Leica SCN 400 slide scanner with an optical magnification factor of 20. With this magnification, the scanner produces images with a spatial resolution of about 0.33×0.33 μm per pixel. The section thickness is approximately 7 μm.

1.2. Aligning Serial Sections

After scanning the immunostained serial section, the images have to be aligned to assemble them back into a volume. This alignment process however poses several challenges.

- The sections are significantly deformed by the cutting knife of the microtome. While small deformations are tolerable for a single section, they need to be corrected for a 3D reconstruction. This means that some non-linear local deformations have to be applied to the scanned slides.
- Removing the embedding material has the consequence that no external markers can be used for the alignment. In contrast to many other applications, it is therefore not possible to use registration markers since they would be lost during staining.
- The specimen is human or animal tissue scanned at a high resolution. Therefore, the images contain highly repetitive structures – i. e. cells – and pose high demands on the processing algorithms. Among other things, this implies

that gradient domain, block- and feature matching cannot be used directly.

The main contribution of the paper is a novel, feature based registration and alignment algorithm that was specifically designed for immunostained serial sections of tissue. It solves several problems that render classical image registration techniques unsuitable in the context of serial section alignment. It is robust to highly repetitive smaller structures that otherwise lead to erroneous alignments. Using an iterative re-matching of the features, it is able to find correct correspondences for a large number of features and automatically removes outliers. It minimizes the overall deformation of the specimen since we do not align to a single reference slice. Thus it reduces the influence of the cutting-induced distortions in the individual slices.

2. Related Work

Shams et al. [SSKH10] provide an extensive survey of parallelized algorithms for medical image registration. The methods they discuss are however all based on local difference measures and thus not directly suitable for our problem. Similarly, Hill et al. [HBHH01] compared various approaches to register MRI and PET images with CT data.

There are also several books on medical image registration algorithms. Goshtasby [Gos05] gives a very broad overview of the methodology and applications of different techniques. More detailed descriptions of various approaches and a deeper mathematical background are provided by [SWL05, Sch06, HH10]. All of these books explicitly discuss non-rigid registration methods in the context of clinical imaging, i. e. CT, MRI, and PET data. An overview of bioimaging software tools is given by Eliceiri et al. [EBG*12].

2.1. Registration of Serial Sections

Only few methods to align serial sections of tissue exist. Among these are manual alignment techniques [vKTVHW85, SRB03]. This approach was later improved by Steiniger et al. [SBS11] using a joystick as input device.

One of the first practical approaches was the ICP algorithm [BM92]. Several semi-automatic approaches for the registration of immunostained serial sections of human capillaries in tumors targeting CD34 [GWM*05, GvdLP*06] were proposed. After an approximate manual pre-alignment using a rigid transformation, an affine transformation is computed, that minimizes the pixel-wise normalized cross-correlation. These are however only suitable for small regions due to the pure linear correction and for small series because of the manual pre-alignment.

A fully automatic approach was proposed by Ourselin et al. [ORS*01] that is based on block matching. Nikou et al. [NHN*03] minimize a global energy function for autoradiography sections, however, they operate on a very small MRT data sets. Ma et al. [MLW*08] developed a method to align sections of a mouse lymph node. It is based on first globally aligning a binary image generated by a foreground/background segmentation. Then a multi-resolution algorithm is used to refine the rigid alignment. A similar approach was proposed by Tanacs and Kato [TK11] for MRT images. Ju et al. [JWC*06] utilize the continuity of the biological matter to reduce "jitter" in the registration of a slide series with warp filtering.

As Steiniger et al. already noted: "Slight distortions of the single sections during the cutting process (and other reasons) led to an irregular outline of the vessels" [SRB03]. Rigid-only registration was studied in context of MRI and similar kinds of data [RPMA01, JS01, MBNV04].

2.2. Non-rigid Registration

Cifor et al. [CBP11] register 2D histological scans using the smoothness assumption: the surface-to-reconstruct is a biological artifact that should not have non-continuous jumps. The elastic method is a quite popular approach [GBB*01, CBR*11]. Gefen et al. [GTN03] use a 3D wavelet to elastically transform histological images. Bajcsy and Kovačič [BK89] developed a multi-resolution elastic algorithm to register CT data sets. Saalfeld et al. [SFCT12] use a 2D elastic triangulation of Hookean springs for block matching. Wirtz et al. [WPFS05] use higher-order image derivatives. Thirion [Thi98] used a diffusion model based on thermodynamic concepts to register two images. Bagci et al. [BCU12] review the modern state of the art approach based on multi-resolution methods. All multi-resolution methods however require data containing large structures which are not present in our specimen.

Rueckert et al. [RSH*99] developed a non-rigid registration of 3D models, especially breast MRTs. It is similar to our work as it also uses a B-spline based deformation. The matching is however based on the mutual information of the images [WVA*96, PLD05] and thus requires clear edges and larger uniform areas in the images. This approach was further improved to utilize multi-level B-splines [SRQ*01]. This allows simulating a non-uniform control point grid, but the similarity measure is still not suitable for our context. Compared to Xie and Farin [XF04], our work features orders of magnitude larger data sets with comparable execution time.

Chui and Rangarajan [CR03] developed an algorithm for non-rigid registration of medical data sets, especially CT/MRT data. They also include a survey on different registration methods in their work. Their method circumvents the matching problem by reformulating the registration as point cloud matching of the features. This idea however does not work in our case, because the point cloud formed by the features is a dense random point set without much structural information. In the context of CT data the results of the EMPIRE10 challenge are of interest [MvGR*11].

Wan et al. [WBDM13] also use feature detection based on SURF and thin-plate splines for the non-rigid registration of a set of synthetic brain MRI images. This method however requires an exhaustive training step for feature selection and thus cannot be used for "one-shot" specimen in the context of medical research. Kim et al. [KBFM97] utilize thin-plate splines for alignment of auto-radiography images. They used a low-resolution undistorted video feed as guide images. Again, large structures are required for this method. In contrast to Auer et al. [ARH05] we operate on much larger images – complete histological scans at 20× magnification. Auer et al. combine a multi-resolution rigid registration with thin-plate spline non-rigid step. We use one-step rigid transform and a B-spline-based non-rigid step. Song et al. [STBM13] register a set of immunostained sections with alternated different staining.

Existing methods all rely on a reference slice to which all others are deformed. As shown by Bagci and Bai [BB10], selecting the "best" reference is crucial for the final result. In contrast to that, we perform a global optimization step to minimize the energy of the non-linear distortions of all slides.

2.3. General Image Registration

There is an extensive research on image registration and its various applications. Early works [LK81] date back more than 30 years ago. Friston et al. [FAF*95] describe the image registration process as a least-squares problem where the differences between images are minimized. Several surveys on image registration methods exist [Bro92, ZF03]. Image registration, as a process of overlaying different images of the same or similar objects typically consists of four phases: feature detection, feature matching, estimation of the transformation, application of the transformation. In our case we first estimate the rigid transformation and then the non-rigid one.

2.4. Feature Detection and Matching

Numerous image feature detection algorithms exist. Recent algorithms detect scale and rotation invariant features. Among them are the SIFT features [Low04], SURF is their improvement in term of run-time efficiency [BETV08]. BRISK [LCS11] aims to further reduce run-time compared to SURF without sacrificing the detection quality. Due to the low run-time and memory consumption, we chose to use this detector in our work. Further feature detectors can be found in the survey of Heinly et al. [HDF12]. The *n*-SIFT [CH09] is a generalization of SIFT to volume and otherwise multi-dimensional data. *n*-SIFT can be used in the registration of multiple volume data sets against each other.

After the features are detected, they need to be matched in pairs between two images. Typically, each feature is matched with the most similar one in the other image. Despite pruning strategies, like only keeping pairs where the matching in the other direction is the same, some mismatches almost always remain. These are usually filtered out using the random sample consensus algorithm [FB81] or one of its variants.

3. Overview

The overall registration and alignment algorithm is split into three steps. First, we determine suitable features in all scanned sections. Then we use those features to perform an initial pairwise rigid alignment of all sections. This alignment is used to iteratively deform the images and to identify the feature correspondences. The non-rigid alignment is performed in such a way, that the overall deformation of the images is minimized. Minimizing the deformation leaves an overall rigid transformation of the images as only degree of freedom. We fix this by preventing rotation and translation of the first slice. This means that the remaining ones are rigidly aligned to the first, but all of them are deformed. This does *not* mean that the first slide is used as a reference for the distortion of all other slides. Finally, the deformed images are generated, forming an aligned stack. Figure 2 shows the overall work flow of our method.

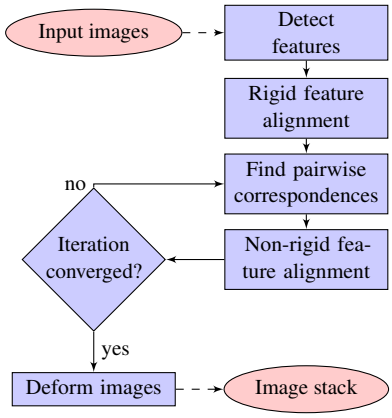

Figure 2: Overall work flow of our non-rigid registration and alignment algorithm.

4. Initial Rigid Alignment

The purpose of the initial rigid alignment step is to roughly register the slices and to facilitate the non-rigid alignment. First, we need to choose adequate feature candidates and then perform a pairwise matching. Based on these matches that still contain a high number of outliers, we then calculate a robust alignment.

4.1. Choosing Candidate Features

The first step we perform for each input image, is finding all feature points. The slides have been normalized prior to feature detection. For this purpose, we use the BRISK feature

detector [LCS11]. Unfortunately, we cannot directly use the detected features and compute pairs by searching for the most similar one in the reference image as shown in Figure 3. The reason for this is that many small features cannot be reliably used because they originate from single cells or other common structures.

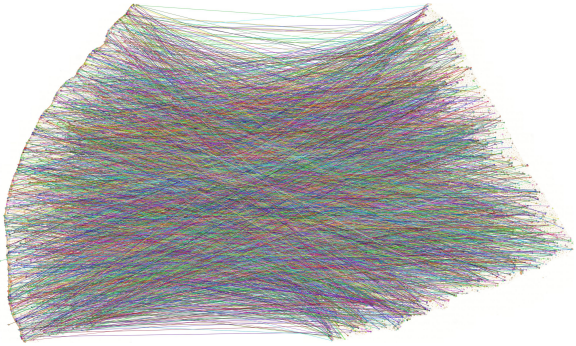

Figure 3: Using standard image registration results in almost random matches due to ambiguous features. Every 10^{th} match is shown only to reduce visual clutter.

On the other hand, larger features – about an order of magnitude larger than a single cell – are usually much less ambiguous. Therefore, we select the N_{select} features in each input image i whose descriptors have the largest diameters. Then we compute pairs by selecting the most similar feature in the reference image $i-1$. The possible candidates can again be reduced by exploiting the fact that there is not much scaling between structures in adjacent sections. Thus we only consider features with a similar descriptor diameter.

$$\frac{1}{1+\varepsilon_l} \leq \frac{d_{tgt}}{d_{ref}} \leq 1+\varepsilon_l, \tag{1}$$

where d_{tgt} and d_{ref} are the target and reference diameters respectively, and the threshold ε_l the maximum local stretch. Figure 4 shows the matches found when only using larger features. Although the quality improved, the matches still contain a high amount of outliers and we have to perform a robust alignment procedure.

4.2. Pairwise Alignment

After finding initial pairs, we perform a random sample consensus (RANSAC) [FB81] based registration. A rigid transformation in 2D is defined by two points and their movement. Actually, this has one degree of freedom more than a rigid transformation because the distance of points cannot change. Since we know that the distance between two corresponding point pairs on neighboring sections can only change due to deformation of the specimen, we can restrict the candidate set. We choose two random matches a and b, and only use

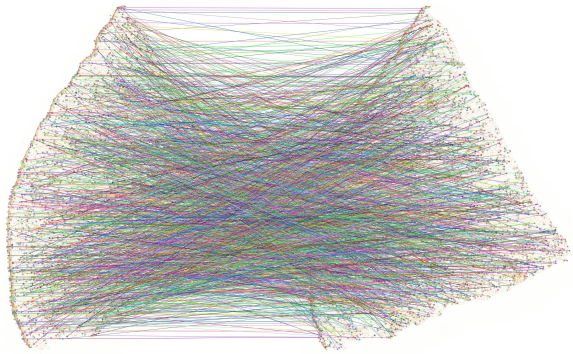

Figure 4: The relative number of false matches is reduced using larger features only. Nevertheless, still many outliers exist. As before, we show only each 10^{th} match to reduce visual clutter.

this pair, if

$$\frac{1}{1+\varepsilon_g} \leq \frac{\|P_{a,tgt}-P_{b,tgt}\|}{\|P_{a,ref}-P_{b,ref}\|} \leq 1+\varepsilon_g \tag{2}$$

$$\|P_{a,tgt}-P_{b,tgt}\| \geq d_{min}\cdot s_{image} \tag{3}$$

$$\|P_{a,ref}-P_{b,ref}\| \geq d_{min}\cdot s_{image}, \tag{4}$$

where $P_{a,tgt}$ is the position of a in the target image, etc., ε_g the maximum global stretch, with $\varepsilon_g \leq \varepsilon_l$, s_{image} the image size, and d_{min} the minimum relative distance between the points. Based on the selected pair, we compute a candidate transformation $\mathbf{R}_i$.

In addition to quickly rejecting futile candidates, we also augment computing the consensus score with the matching score of the pairs that are determined as inliers for the given transformation. Instead of simply counting all matches j with $\|\mathbf{R}_i P_{j,tgt} - \mathbf{R}_{i-1} P_{j,ref}\| \leq s_{image}\cdot\varepsilon_g$, we accumulate

$$\frac{1}{1+w_{match}\delta_j}, \tag{5}$$

where δ_{match} is the difference of the descriptors and w_{match} a weighting constant.

After finding a good transformation using the RANSAC algorithm, we again compute the inlier set. From this, we compute a rigid transformation with a weighted least squares error. The weighting is the same that we already used to compute the consensus score (see Equation 5). Figure 5 shows the found rigid transformation between two sections together with the matches in the consensus set.

5. Non-rigid Alignment

The non-rigid alignment is an iterative process because each deformation of the images may change the inlier/outlier classification and thus the matching pairs. We first start by finding a corresponding feature in the reference images. Then

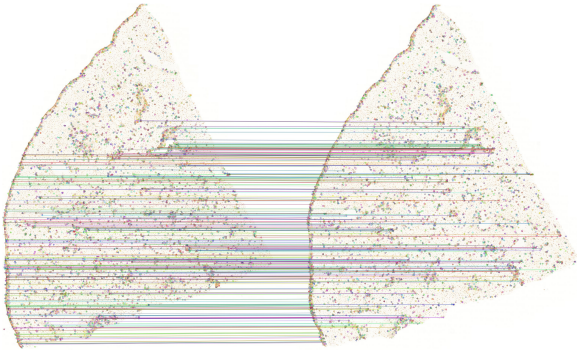

Figure 5: Rigid registration between two sections with the consensus set of matching features. Notice that the upper area cannot be aligned due to local deformations.

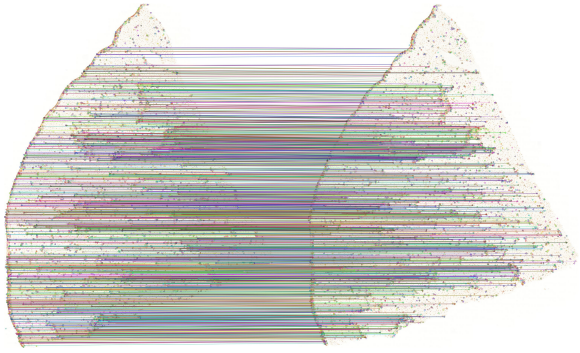

Figure 6: Pairwise matches found in the first iteration, where only high confidence matches – i.e. weight ≥ 0.2 – are shown. Note that despite the increased density of matches, there are still very sparsely covered regions where large deformations are present, e.g. at the top of the image.

we perform a least-squares deformation trying to align all found pairs. Finally, we compute the feature positions after deformation and check if the matches are still valid or if we can find a better correspondence that is now within the local search radius. If all pairs remain – or if we have performed a maximum number of iterations it_{max} – the registration terminates. We do not select a reference slide and deform all slides to match it, but rely on global optimization to minimize the energy of the deformation.

5.1. Finding Pairwise Matches

In each iteration, we first start finding new matches. For each feature j in image i we search a corresponding feature k in image $i-1$ with the most similar descriptor under the constraint that

$$\| T_i\left(P_{j,i}\right) - T_{i-1}\left(P_{k,i-1}\right) \| \leq s_{image} \cdot \varepsilon_g, \tag{6}$$

where T_i is the non-rigid transformation of image i. Note that in the first iteration, this is the rigid transformation $\mathbf{R}_i$. Figure 6 shows the matches found in the first iteration.

5.2. Computing Image Deformations

The non-linear deformation is based on a uniform bi-cubic B-spline over a 9×9 control point grid with three additional control points outside the image. The control point net initially covers the first image. The aligned images are constructed in the parameter domain of the B-spline that is scaled such that it has the same size as the first input image. This means that we can simply evaluate the B-spline to compute the source position in the deformed image for each pixel of the output.

We register each image to the previous one, starting with the registration of the second to the first. For each matching feature pair j,k in image i and $i-1$ respectively, we have the following constraint of the control points:

$$\sum_{l=0}^{14}\sum_{m=0}^{14} B_l(u)B_m(v)\alpha^i_{l,m} = \mathbf{R}_i P_{j,i}, \tag{7}$$

$$u_i = u\left(T_i(P_{j,i})\right) \quad v_i = v\left(T_i(P_{j,i})\right), \tag{8}$$

where u and v are the mappings of a pixel in the aligned image to the parameter values, and $\alpha^i_{l,m}$ are the control points of the B-spline of image i. Again, we use the same confidence weighting described in Equation 5.

In addition, we want to prevent large deformations and smooth areas where we have no matches. We achieve this by adding a constraint for each edge of the control meshes:

$$\left(\alpha^i_{l+1,m} - \alpha^i_{l,m}\right) w_\alpha = \begin{pmatrix} d_x \\ 0 \end{pmatrix} \tag{9}$$

$$\left(\alpha^i_{l,m+1} - \alpha^i_{l,m}\right) w_\alpha = \begin{pmatrix} 0 \\ d_y \end{pmatrix}, \tag{10}$$

where d_x and d_y are the distances between two neighboring control points in the output image in x and y direction and w_α is the smoothing weight. Note that this also induces a penalty for rotations but this is unproblematic because we already performed a global rigid alignment.

Combining all of the constraints leads to a sparse linear equation system. We solve this using the conjugate gradient method [PTVF07] for sparse matrices. As initial value we use the control points from the previous iteration. For the first iteration, we simply set $\alpha^i_{l,m} = ((l-3)d_x, (m-3)d_y)^T$ which is a non-deformed control grid.

As the first image is not deformed, this leaves an overall deformation of all images as a degree of freedom. We use this to minimize the mean square deformation of all images after each registration pass. Moving each control point of all images by the same offset does not change the matching. We can thus minimize the mean square deformation by moving

the control points, such that the average of each control point l,m over all images (including the first one) lies on a grid. In other words, we constrain the control points such that:

$$\sum_{i=1}^{N_{img}} \alpha^i_{l,m} = \begin{pmatrix} (l-3)d_x \\ (m-3)d_y \end{pmatrix}. \tag{11}$$

This uses the remaining degrees of freedom in the alignment to force the "average deformation" to be zero. Previous approaches simply fixed a reference slice such that it was not deformed at all.

5.3. Deforming the Images

To deform the images, we use the OpenCV [Bra00] function `remap`. First, we compute the position in the source image for each pixel of the output image and store it in an array. Instead of evaluating the complete B-spline function for each pixel, we can exploit the fact that the image is a uniform grid. For each row of control points, we evaluate the 1D cubic B-spline for the x-coordinate of each pixel. Then we only need to compute 1D cubic B-splines instead of bicubic B-splines per pixel. As the number of image lines is significantly higher than the number of control point rows we only need to compute 4 basis functions instead of 8 per pixel and accumulate 4 instead of 16 control points. In total, this roughly saves 70% of the computation time. Then, the computed pixel location array is used to generate the aligned image. For the reconstruction, we use bi-linear filtering.

6. Results

Figure 7 shows an overview of the complete data set of the human spleen specimen consisting of 24 sections with a resolution of 25856×32000 pixels each. The thickness of each section is approximately 7 μm, so the digitized specimen has a total thickness of about 170 μm. The image is generated using a volume renderer that combines all sections into a single thick specimen. Such view would be impossible without the registration.

Figure 8 shows two interesting areas of the spleen specimen. On the left, it shows the shape of a larger artery, dividing up further until the capillaries, and the right side shows the blood supply of a follicle. Single sections do not contain longer portions of blood vessel, as Figure 1, second image, visually depicts. On a larger scale, the shape of the capillary network in the spleen can be reconstructed from our volume data using standard visualization algorithms like marching cubes (third image).

6.1. Alignment

The complete registration and alignment pipeline is implemented in C++ using the OpenCV Library [Bra00] version 2.4.8. The run-times are measured on an Intel Core i7 with 16 GB of RAM running Windows 7 64 bit and the executable

Figure 7: Overview of the complete aligned data set of the human spleen specimen. Capillary and larger vessel endothelia and certain fibroblasts are colored brown, visualizing the vascular network.

is also compiled as 64 bit. We use the following constants for the alignment:

- Number of features selected per image $N_{select} = 20,000$
- Minimum RANSAC edge length $d_{min} = 0.1$
- Maximum local deformation $\varepsilon_l = 0.01$
- Maximum global deformation $\varepsilon_g = 0.005$
- Descriptor weight for matches $w_{match} = 10$
- Maximum number of non-rigid iterations $it_{max} = 20$
- Smoothing weight $w_\alpha = 0.2$

The final matches found for the alignment of two sections are shown in Figure 9. Matching feature pairs have been found for the whole area.

In our experiments we also encountered teared or otherwise damaged slides. Because of our global optimization approach it was possible to register the batch with sufficient accuracy. The final aligned data set is shown in Figure 1, right. Although the damage was not "repaired" by our method, it is robust enough to align all parts.

Figure 10 compares our registration with the standard ICP algorithm [BM92]. We used the implementation of Pomerleau et al. [PCSM13]. Starting from the original images, the ICP algorithm converges to a local minimum (top left). Using

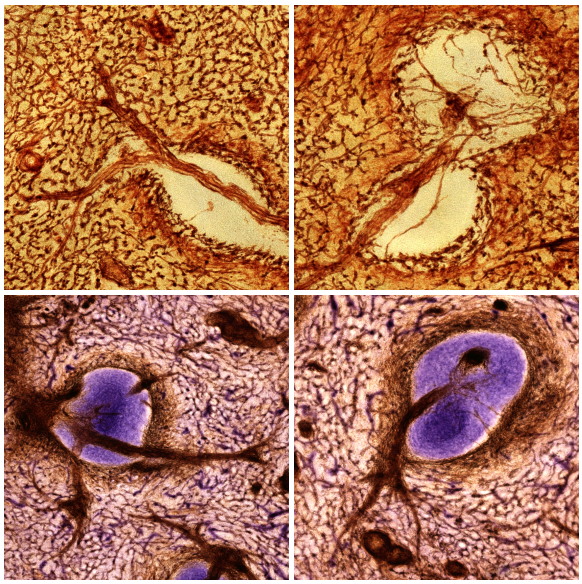

Figure 8: In the top left a larger artery develops into a network of smaller vessels. The shape of the blood vessel network in human spleens is unexplored, except for the fact that it has open ends. The top right image shows the blood supply of a lymphatic follicle. The bottom images show similar structures in the two-color specimen. Such in-depth views of were impossible so far.

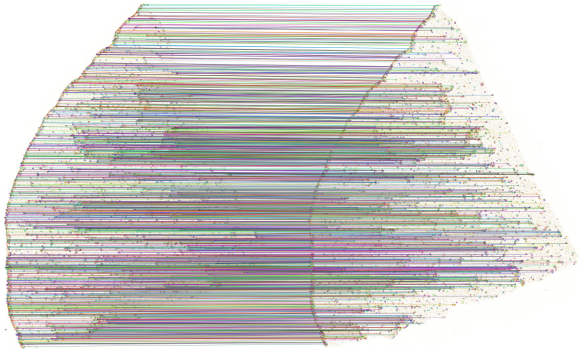

Figure 9: Final matches found during alignment of two sections, where only high confidence matches – i. e. weight ≥ 0.2 – are shown. The whole images are densely covered with correctly matched feature pairs.

a manual pre-alignment, it obtains better results (top right). Due to the ambiguities, caused by the repetitive structures in human tissue, a consecutive non-rigid alignment, e. g. using the method of Chui and Rangarajan [CR03] cannot correctly align the scans. In contrast to that, our method achieves much better results on the same data with the rigid stage only (bottom left). The final non-rigid stage (bottom right) drastically improves the alignment.

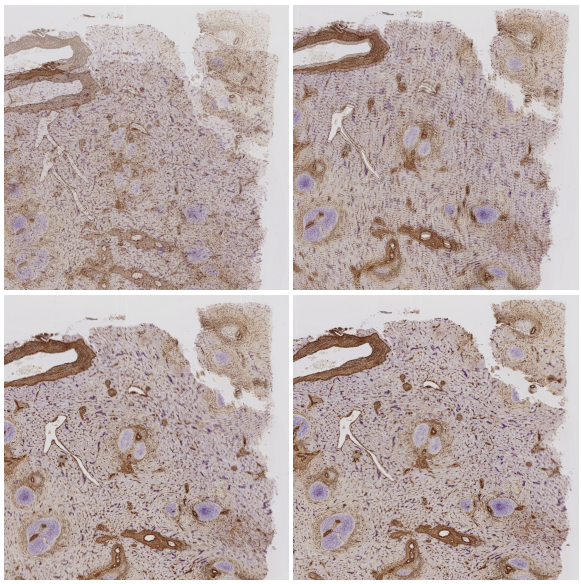

Figure 10: Alignment comparison showing the upper right corner of two consecutive spleen sections stained for CD34 and smooth muscle alpha actin in brown, and for CD271 in blue. Top left: result of the ICP algorithm applied to the original images. Top right: ICP with initial manual positioning of the sections. Bottom left: result of our rigid registration. Bottom right: the result of our non-rigid registration (final output of our method).

Table 1 shows the timings for the different steps of the algorithm. The initial number of features detected per image is between 430k and 450k, so we keep the 4–5% largest ones. Despite the iterative non-rigid alignment procedure, the actual deformation of the images requires most of the time. This is due to the fact, that the bi-cubic B-spline has to be evaluated for every pixel of the output images. Note that using thin plate splines, this step would take significantly longer due to the high number of matched features. The run times for both data sets were identical since the images have the same size and both contain 24 slides. Due to the pairwise matching and the sparse linear system, our method is linear in the number of slides.

time (mm:ss)	feature detection	rigid transf.	non-rig. transf.	image recon.
image[a]/pair[b]	0:42[a]	0:08[b]	1:03[b]	1:17[a]
total	16:58	3:20	24:02	30:35

Table 1: Execution times for the spleen data sets with 24 sections. The first line shows the average time for various phases of our method that is required per image or pair. The second line shows total time for each phase.

7. Conclusion and Limitations

After aligning stacks of immunostained spleen serial sections, we have produced volume renderings of two different specimen, as well as a 3D-model of the vessels (Figures 1 and 7). These enable the domain experts to analyze and discuss the shape and function of capillaries and arterial blood vessels in the spleen at a level impossible without our method. Details of interesting areas already discovered are shown in Figure 8.

To achieve this goal, we have presented a method that is able to robustly register and align immunostained serial sections. This is an especially challenging task due to the highly repetitive cellular structures in the tissue. Our algorithm tolerates relatively large local and global deformations. We measured a global deformation of up to 2% of the image diagonal and a local stretch of up to 5%.

The most time consuming part of our method is the reconstruction of the deformed images. Therefore, we plan to implement this step on the GPU in the future. A second candidate for a GPU implementation is the conjugate gradient solver which needs most of the time in the non-rigid alignment phase.

Although we have developed and used our approach for human spleen specimens, it is much more widely applicable. Due to the use of feature detection to find similar structures in adjacent sections, our approach is only limited to tissue that contains at least some special histological structures. At a mesoscopic scale this is however no limitation, as blood vessels always provide sufficient landmarks in human organs.

While our method appears to be robust even to teared or damaged slides, explicitly repairing the damage before alignment would have several advantages. The alignment will be more precise close to the fracture as there will be consistent feature pairs on both sides. On the other hand, the reconstructed volume will also not be fractured any more. We therefore want to develop a method to find and "repair" the fractures in the scanned slides.

Acknowledgments

We would like to thank Anja Seiler and Kathrin Lampp from Philipps-University Marburg for producing the sections and performing the immunostaining. In addition, we thank Sandra Iden and Astrid Schauss from the CECAD Cluster of Excellence at University Cologne and Verena Wilhelmi from Philipps-University Marburg for helping a lot with the image acquisition.

References

[ARH05] AUER M., REGITNIG P., HOLZAPFEL G.: An automatic nonrigid registration for stained histological sections. *IEEE T. Image Process. 14*, 4 (2005), 475–486. 4

[BB10] BAGCI U., BAI L.: Automatic best reference slice selection for smooth volume reconstruction of a mouse brain from histological images. *IEEE Trans. Med. Imaging 29*, 9 (2010), 1688–1696. 4

[BCU12] BAGCI U., CHEN X., UDUPA J.: Hierarchical scale-based multiobject recognition of 3-D anatomical structures. *IEEE Trans. Med. Imaging 31*, 3 (2012), 777–789. 3

[BETV08] BAY H., ESS A., TUYTELAARS T., VAN GOOL L.: SURF: Speeded Up Robust Features. *Comput. Vision Image Understanding 110*, 3 (2008), 346–359. 4

[BK89] BAJCSY R., KOVAČIČ S.: Multiresolution elastic matching. *Comput. Vis. Graph. Image Process. 46*, 1 (1989), 1–21. 3

[BM92] BESL P. J., MCKAY N. D.: A method for registration of 3-D shapes. *IEEE Trans. Pattern Anal. Mach. Intell. 14*, 2 (1992), 239–256. 3, 7

[Bra00] BRADSKI G.: The OpenCV Library. *Dr. Dobb's Journal of Software Tools* (2000). 7

[Bro92] BROWN L. G.: A survey of image registration techniques. *ACM Comput. Surv. 24*, 4 (1992), 325–376. 4

[CBP11] CIFOR A., BAI L., PITIOT A.: Smoothness-guided 3-d reconstruction of 2-D histological images. *NeuroImage 56*, 1 (2011), 197–211. 3

[CBR*11] CHAPPELOW J., BLOCH B. N., ROFSKY N., GENEGA E., LENKINSKI R., DEWOLF W., MADABHUSHI A.: Elastic registration of multimodal prostate MRI and histology via multi-attribute combined mutual information. *Med. Phys. 38*, 4 (2011), 2005–2018. 3

[CH09] CHEUNG W., HAMARNEH G.: *n*-SIFT: *n*-dimensional scale invariant feature transform. *IEEE Trans. Image Process. 18*, 9 (2009), 2012–2021. 4

[CR03] CHUI H., RANGARAJAN A.: A new point matching algorithm for non-rigid registration. *Comput. Vision Image Understanding 89*, 2–3 (2003), 114–141. 3, 8

[EBG*12] ELICEIRI K. W., BERTHOLD M. R., GOLDBERG I. G., IBÁÑEZ L., MANJUNATH B. S., MARTONE M. E., MURPHY R. F., PENG H., PLANT A. L., ROYSAM B., ET AL.: Biological imaging software tools. *Nat. Methods 9*, 7 (2012), 697–710. 3

[FAF*95] FRISTON K. J., ASHBURNER J., FRITH C. D., POLINE J.-B., HEATHER J. D., FRACKOWIAK R. S. J.: Spatial registration and normalization of images. *Human Brain Mapping 3*, 3 (1995), 165–189. 4

[FB81] FISCHLER M. A., BOLLES R. C.: Random sample consensus: A paradigm for model fitting with applications to image analysis and automated cartography. *Commun. ACM 24*, 6 (1981), 381–395. 4, 5

[GBB*01] GUEST E., BERRY E., BALDOCK R., FIDRICH M., SMITH M.: Robust point correspondence applied to two- and three-dimensional image registration. *IEEE Trans. Pattern Anal. Mach. Intell. 23*, 2 (2001), 165–179. 3

[Gos05] GOSHTASBY A. A.: *2-D and 3-D image registration: for medical, remote sensing, and industrial applications*. Wiley, 2005. 3

[GTN03] GEFEN S., TRETIAK O., NISSANOV J.: Elastic 3-D alignment of rat brain histological images. *IEEE Trans. Med. Imaging 22*, 11 (2003), 1480–1489. 3

[GvdLP*06] GILHUIS H. J., VAN DER LAAK J. A., POMP J., KAPPELLE A. C., GIJTENBEEK J. M., WESSELING P.: Three-dimensional (3D) reconstruction and quantitative analysis of the microvasculature in medulloblastoma and ependymoma subtypes. *Angiogenesis 9*, 4 (2006), 201–208. 3

[GWM*05] GIJTENBEEK J. M., WESSELING P., MAASS C.,

BURGERS L., VAN DER LAAK J. A.: Three-dimensional reconstruction of tumor microvasculature: simultaneous visualization of multiple components in paraffin-embedded tissue. *Angiogenesis 8*, 4 (2005), 297–305. 3

[HBHH01] HILL D. L. G., BATCHELOR P. G., HOLDEN M., HAWKES D. J.: Medical image registration. *Phys. Med. Biol. 46*, 3 (2001), R1–R45. 3

[HDF12] HEINLY J., DUNN E., FRAHM J.-M.: Comparative evaluation of binary features. In *Computer Vision – ECCV 2012*, LNCS 7573. Springer, 2012, pp. 759–773. 4

[HH10] HAJNAL J. V., HILL D. L.: *Medical image registration*. CRC press, 2010. 3

[JS01] JENKINSON M., SMITH S.: A global optimisation method for robust affine registration of brain images. *Med. Image Anal. 5*, 2 (2001), 143–156. 3

[JWC*06] JU T., WARREN J., CARSON J., BELLO M., KAKADIARIS I., CHIU W., THALLER C., EICHELE G.: 3D volume reconstruction of a mouse brain from histological sections using warp filtering. *J. Neurosci. Methods 156*, 1–2 (2006), 84–100. 3

[KBFM97] KIM B., BOES J. L., FREY K. A., MEYER C. R.: Mutual information for automated unwarping of rat brain autoradiographs. *NeuroImage 5*, 1 (1997), 31–40. 4

[LCS11] LEUTENEGGER S., CHLI M., SIEGWART R. Y.: BRISK: Binary robust invariant scalable keypoints. In *IEEE Conf. Computer Vision* (2011), ICCV '11, IEEE, pp. 2548–2555. 4, 5

[LK81] LUCAS B. D., KANADE T.: An iterative image registration technique with an application to stereo vision. In *Proc. Intl. Joint Conf. Artificial Intelligence* (1981), IJCAI '81, pp. 674–679. 4

[Low04] LOWE D. G.: Distinctive image features from scale-invariant keypoints. *Int. J. Comput. Vision 60*, 2 (2004), 91–110. 4

[MBNV04] MALANDAIN G., BARDINET E., NELISSEN K., VANDUFFEL W.: Fusion of autoradiographs with an MR volume using 2-D and 3-D linear transformations. *NeuroImage 23*, 1 (2004), 111–127. 3

[MLW*08] MA B., LIN Z., WINKELBACH S., LINDENMAIER W., DITTMAR K. E.: Automatic registration of serial sections of mouse lymph node by using image-reg. *Micron 39*, 4 (2008), 387–396. 3

[MvGR*11] MURPHY K., VAN GINNEKEN B., REINHARDT J., KABUS S., DING K., ET AL.: Evaluation of registration methods on thoracic CT: The EMPIRE10 challenge. *IEEE T. Med. Imaging 30*, 11 (2011), 1901–1920. 3

[NHN*03] NIKOU C., HEITZ F., NEHLIG A., NAMER I. J., ARMSPACH J.-P.: A robust statistics-based global energy function for the alignment of serially acquired autoradiographic sections. *J. Neurosci. Methods 124*, 1 (2003), 93–102. 3

[ORS*01] OURSELIN S., ROCHE A., SUBSOL G., PENNEC X., AYACHE N.: Reconstructing a 3D structure from serial histological sections. *Image & Vision Comput. 19* (2001), 25–31. 3

[PCSM13] POMERLEAU F., COLAS F., SIEGWART R., MAGNENAT S.: Comparing ICP variants on real-world data sets. *Auton. Robot 34*, 3 (Feb. 2013), 133–148. 7

[PLD05] PENG H., LONG F., DING C.: Feature selection based on mutual information criteria of max-dependency, max-relevance, and min-redundancy. *IEEE Trans. Pattern Anal. Mach. Intell. 27*, 8 (2005), 1226–1238. 3

[PTVF07] PRESS W. H., TEUKOLSKY S. A., VETTERLING W. T., FLANNERY B. P.: *Numerical Recipes: The Art of Scientific Computing*, 3 ed. Cambridge University Press, 2007. 6

[RPMA01] ROCHE A., PENNEC X., MALANDAIN G., AYACHE N.: Rigid registration of 3-D ultrasound with MR images: a new approach combining intensity and gradient information. *IEEE Trans. Med. Imaging 20*, 10 (2001), 1038–1049. 3

[RSH*99] RUECKERT D., SONODA L. I., HAYES C., HILL D. L. G., LEACH M. O., HAWKES D.: Nonrigid registration using free-form deformations: application to breast MR images. *IEEE Trans. Med. Imaging 18*, 8 (1999), 712–721. 3

[SBS11] STEINIGER B., BETTE M., SCHWARZBACH H.: The open microcirculation in human spleens: a three-dimensional approach. *J. Histochem. Cytochem. 59*, 6 (2011), 639–648. 3

[Sch06] SCHERZER O. (Ed.): *Mathematical models for registration and applications to medical imaging*. Springer, 2006. 3

[SFCT12] SAALFELD S., FETTER R., CARDONA A., TOMANCAK P.: Elastic volume reconstruction from series of ultra-thin microscopy sections. *Nat. Methods 9*, 7 (2012), 717–720. 3

[SRB03] STEINIGER B., RÜTTINGER L., BARTH P. J.: The three-dimensional structure of human splenic white pulp compartments. *J. Histochem. Cytochem. 51*, 5 (2003), 655–663. 3

[SRQ*01] SCHNABEL J. A., RUECKERT D., QUIST M., BLACKALL J. M., CASTELLANO-SMITH A. D., ET AL.: A generic framework for non-rigid registration based on non-uniform multi-level free-form deformations. In *Medical Image Computing and Computer-Assisted Intervention*, LNCS 2208. Springer, 2001, pp. 573–581. 3

[SSKH10] SHAMS R., SADEGHI P., KENNEDY R., HARTLEY R.: A survey of medical image registration on multicore and the GPU. *IEEE Signal Process Mag. 27*, 2 (2010), 50–60. 3

[STBM13] SONG Y., TREANOR D., BULPITT A., MAGEE D.: 3D reconstruction of multiple stained histology images. *Journal of Pathology Informatics 4*, 2 (2013), 7. 4

[SWL05] SURU J. S., WILSON D. L., LAXIMINARAYAN S.: *Handbook of biomedical image analysis*, vol. 3. Springer, 2005. 3

[Thi98] THIRION J.-P.: Image matching as a diffusion process: an analogy with Maxwell's demons. *Med. Image Anal. 2*, 3 (1998), 243–260. 3

[TK11] TANACS A., KATO Z.: Fast linear registration of 3D objects segmented from medical images. In *Conf. Biomedical Engineering and Informatics* (2011), BMEI '11, pp. 294–298. 3

[vKTVHW85] VAN KRIEKEN J. H., TE VELDE J., HERMANS J., WELVAART K.: The splenic red pulp; a histomorphometrical study in splenectomy specimens embedded in methylmethacrylate. *Histopathology 9*, 4 (1985), 401–416. 3

[WBDM13] WAN T., BLOCH B. N., DANISH S., MADABHUSHI A.: A novel point-based nonrigid image registration scheme based on learning optimal landmark configurations. In *Medical Imaging 2013: Image Processing* (2013), Proc. SPIE 8669, pp. 866934–866934–12. 4

[WPFS05] WIRTZ S., PAPENBERG N., FISCHER B., SCHMITT O.: Robust and staining-invariant elastic registration of a series of images from histologic slices. In *Proc. SPIE* (2005), Proc. SPIE 5747, pp. 1256–1262. 3

[WVA*96] WELLS III W. M., VIOLA P., ATSUMI H., NAKAJIMA S., KIKINIS R.: Multi-modal volume registration by maximization of mutual information. *Med. Image Anal. 1*, 1 (1996), 35—51. 3

[XF04] XIE Z., FARIN G.: Image registration using hierarchical B-splines. *IEEE Trans. Visual Comput. Graphics 10*, 1 (2004), 85–94. 3

[ZF03] ZITOVÁ B., FLUSSER J.: Image registration methods: a survey. *Image & Vision Comput. 21*, 11 (2003), 977–1000. 4